


Methanol-to-Olefin Conversion on Silicoaluminophosphate Catalysts: Effect of Brønsted Acid Sites and Framework Structures

Weili Dai,^{†,‡} Xin Wang,[†] Guangjun Wu,[†] Naijia Guan,[†] Michael Hunger,[‡] and Landong Li^{*,†}

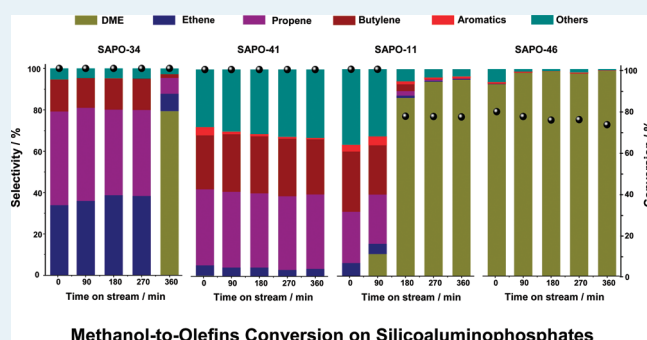
[†]Key Laboratory of Advanced Energy Materials Chemistry (Ministry of Education), College of Chemistry, Nankai University, Tianjin 300071, P.R. China

[‡]Institute of Chemical Technology, University of Stuttgart, 70550 Stuttgart, Germany

 Supporting Information

ABSTRACT: Silicoaluminophosphates (SAPO) with different framework structures and amounts of Brønsted acid sites, that is, SAPO-34, SAPO-41, SAPO-11, and SAPO-46, were synthesized and studied as catalysts for the methanol-to-olefin (MTO) conversion. Besides the well-known SAPO-34 catalyst, also SAPO-41 exhibits a good MTO performance with a methanol conversion of 100% and a selectivity to light olefins of about 70% at the reaction temperature of 723 K, which maintains up to a time-on-stream of 10 h. The Brønsted acid sites of silicoaluminophosphate catalysts employed in this study were characterized by means of ¹H MAS NMR spectroscopy. These studies were performed with unloaded samples for studying the type and number of OH groups and after loading of ammonia for determining the amount of accessible Brønsted acid sites. The occluded organic species formed on the catalysts during the MTO reaction were analyzed by in situ UV/vis spectroscopy, thermogravimetry-differential thermal analysis (TG-DTA), and gas chromatography-mass spectrometry (GC-MS). On the basis of the characterization and catalytic results, we discuss the effects of Brønsted acid sites and framework structures on the catalytic performance of silicoaluminophosphates in the MTO conversion. The amount of Brønsted acid sites strongly affects the adsorption of methanol and the formation of hydrocarbon pool compounds as well as the catalyst deactivation. On the other hand, the framework structures of the silicoaluminophosphates under study influence the diffusion of products and thus control the product selectivity of the MTO reaction.

KEYWORDS: MTO, silicoaluminophosphate, framework structure, Brønsted acid sites, hydrocarbon pool compounds



1. INTRODUCTION

Light olefins are quite important components for the petrochemical industry, and the market demand for light olefins is growing steadily in recent years. Conventionally, light olefins are produced by thermal cracking or catalytic cracking of crude oil. However, because of the rapid increase in the price of crude oil and the shortage in the foreseeable future, alternative routes for the production of light olefins from non-oil sources are desired and thereby, the methanol-to-olefin (MTO) conversion on microporous solid acids is drawing more and more attention.^{1–3} In the MTO process, methanol is dehydrated to dimethyl ether (DME) and the obtained equilibrium mixture consisting of methanol, DME, and water is converted to light olefins after a kinetic induction period. The light olefins thereafter react to paraffins, aromatics, naphthenes, and higher olefins via hydrogen transfer, alkylation, and poly condensation.³ The general feature of this reaction is accepted as a hydrocarbon pool mechanism described as a catalytic scaffold composed of large olefinic compounds and cyclic organic species contained in the cages or channels of microporous solid acids. The reactants methanol and DME are repeatedly added to these hydrocarbon pool

compounds, while light olefins are formed and eliminated in a closed cycle.^{4,5}

A variety of acidic microporous catalysts have been studied as possible MTO catalysts. The acidity and framework structure are two key factors controlling the catalytic performances of these materials. The silicoaluminophosphate SAPO-34 with Brønsted acid sites of moderate acid strength and a well-defined framework with large cages and 8-ring windows is reported to be most promising catalyst giving a maximum light olefin (propene and ethene) yield of up to 80%.⁶ The catalytic and mechanistic aspects of the MTO reaction on SAPO-34 have been extensively studied.^{6–16} Specifically, polyalkylaromatics confined inside the cages of SAPO-34 (diameter of ca. 9.4 Å) have been found as the most active hydrocarbon pool compound causing the formation of light olefins upon activation by Brønsted acid sites at the inorganic framework.¹⁰ The small 8-ring windows (diameter of ca. 3.8 Å, entrances to the cages) restrict the diffusion of heavy

Received: January 13, 2011

Revised: February 10, 2011

Table 1. Parameters of the Synthesis of the Silicoaluminophosphates under Study

sample	batch composition ^a	temperature/ time/		
		K	h	ref
SAPO-34	1Al ₂ O ₃ :1P ₂ O ₅ :0.5SiO ₂ :2TEA:50H ₂ O	473	24	23
SAPO-41	1Al ₂ O ₃ :1P ₂ O ₅ :0.2SiO ₂ :4DPA:50H ₂ O	473	96	24
SAPO-11	1Al ₂ O ₃ :1P ₂ O ₅ :0.5SiO ₂ :2Pr ₂ NH:50H ₂ O	473	48	25
SAPO-46	1Al ₂ O ₃ :1P ₂ O ₅ :0.5SiO ₂ :4DPA:50H ₂ O	473	72	24

^a Molar ratio.

and branched hydrocarbons and, therefore, lead to a high selectivity to the desired light olefins. Moreover, the Brønsted sites of SAPO-34 with moderate acid strength, in comparison to the aluminosilicate analogue SSZ-13, result in better resistance to coking and, therefore, a longer lifetime in the MTO reaction.¹⁶

Initiated by the success of SAPO-34, other silicoaluminophosphates were explored as alternative MTO catalysts. These studies have been focused especially on silicoaluminophosphates with small entrances to large cages, for example, SAPO-18^{17–20} and SAPO-35.^{6,21} More recently, the silicoaluminophosphate STA-7 (SAV) built up by large cages, similar to SAPO-34, has been reported to be a good catalyst for the MTO reaction.²² Silicoaluminophosphates with one-dimensional pore systems and no cages, for example, SAPO-11,^{19,21} on the other hand, have been reported to be not good catalysts for the MTO conversion.

In the present study, several types of silicoaluminophosphates with different amounts of Brønsted acid sites and various framework structures having very different pore systems were synthesized and applied as MTO catalysts, or more generalized, for the MTH (methanol-to-hydrocarbons) reaction. The amounts of Brønsted acid sites of the silicoaluminophosphates under study were determined by means of ¹H MAS NMR spectroscopy. SAPO-34 and SAPO-46 both possess structures with cages. In contrast, SAPO-11 and SAPO-41 are characterized by structures with one-dimensional 10-ring pore systems, while the amounts of Brønsted acid sites of these catalysts are obviously different. The aim of this investigation is to improve our understanding of the relationship between framework properties (type and number of Brønsted acid sites, methanol adsorption capacity, and pore structure) and the catalytic behavior (selectivity to olefins and deactivation) of silicoaluminophosphate catalysts applied for the MTO reaction.

2. EXPERIMENTAL SECTION

2.1. Synthesis of Silicoaluminophosphates. All the silicoaluminophosphates were prepared via hydrothermal methods following the procedures in the literature.^{23–25} The as-synthesized materials were calcined in air at 873 K for 4 h to remove the occluded organic structure-directing-agents. The chemical compositions of the synthesis mixtures and the conditions for the synthesis of silicoaluminophosphates are summarized in Table 1.

2.2. Characterization of Silicoaluminophosphates. X-ray diffraction (XRD) patterns of the as-synthesized products were recorded on a Bruker D8 diffractometer with CuK α radiation ($\lambda = 1.5418 \text{ \AA}$) from 5 to 50° with a scan speed of $2\theta = 6.0^\circ/\text{min}$. A HITACHI S-4700 Scanning Electron Microscope (SEM) was used for the studies of the silicoaluminophosphate morphologies. The SEM images were recorded on samples covered with a thin layer of gold, deposited by sputtering. The surface areas of the catalysts were obtained by means of nitrogen adsorption

measurements performed at 77 K on a Quantachrome Autosorb 3B instrument. Before N₂ adsorption, the samples were dehydrated at 473 K for 2 h. The total surface area was calculated via the Brunauer–Emmett–Teller (BET) equation. The chemical compositions of the calcined silicoaluminophosphates were determined by ICP-AES.

¹H and ²⁹Si MAS NMR spectra were recorded on a Bruker Avance III spectrometer at resonance frequencies of 400.1 and 79.5 MHz, with $\pi/2$ and $\pi/4$ single pulse excitation, repetition times of 10 and 20 s, and using 4 mm and 7 mm MAS NMR probes with sample spinning rates of 8.0 and 4.0 kHz, respectively. The samples used for the ¹H MAS NMR studies were dehydrated at 723 K in vacuum (pressure below 10⁻² Pa) for 12 h. After dehydration, the samples were sealed and kept in glass tubes until they were filled into the MAS NMR rotors in a glovebox purged with dry nitrogen gas. The determination of the number of accessible Brønsted acid sites was performed by adsorption of NH₃ at room temperature. After the NH₃ loading, the samples were evacuated at 453 K for 2 h to eliminate physisorbed ammonia. Quantitative ¹H MAS NMR measurements were performed by comparing the signal intensities of the samples under study with the intensity of an external intensity standard (dehydrated zeolite HNa-Y with the cation exchange degree of 35%). All chemical shift values were referenced to tetramethylsilane (TMS). The decomposition and simulation of NMR spectra were carried out using the Bruker software WINFIT.

2.3. Methanol Adsorption on Silicoaluminophosphates. Isotherms of methanol adsorption on silicoaluminophosphates were measured at 298 K using an intelligent gravimetric analyzer (IGA-002, Hiden Isochema Instrument) with a sensitivity of 0.1 μg . The apparatus is an ultrahigh vacuum system for recording isotherms and determining the corresponding adsorption kinetics by setting pressure steps. Before the adsorption measurements, the calcined samples were degassed at 383 K overnight.

2.4. MTO Reaction over Silicoaluminophosphates. The MTO reaction was performed in a fixed-bed reactor at atmospheric pressure. Typically, a 0.4 g sample (sieve fraction, 0.25–0.5 mm) was placed in a stainless steel reactor (5 mm i.d.) and activated under flowing N₂ at 723 K for 1 h. Methanol was pumped in at 0.5 mL/h (WHSV = 1/h) at 473 K. The products were analyzed online by gas chromatography equipped with a flame ionization detector and a packed-column Porapak Q to separate the C₁–C₈ hydrocarbons. The temperature of the column was maintained at 313 K for 15 min and then increased to 473 K with a heating rate of 10 K/min.

2.5. In Situ UV/vis Studies of the MTO Reaction on Silicoaluminophosphates. The composition of the hydrocarbon pool compounds formed under reaction conditions was studied by in situ UV/vis spectroscopy using a fiber-optic UV/vis²⁶ (see Supporting Information, Figure S1). Reference UV/vis spectra of silicoaluminophosphates were recorded at reaction temperature prior to starting the methanol flow. UV/vis spectra at 200 to 600 nm in the diffuse reflection mode were conducted with a AvaSpec-2048 Fiber Optic spectrometer, an AvaLight-DH-S deuterium light source by Avantes, and a glass fiber reflection probe HPSUV1000A by Oxford Electronics.

2.6. Characterization of Occluded Organic Compounds on Silicoaluminophosphates. The amounts of occluded hydrocarbons after the methanol reaction were analyzed by thermogravimetry-differential thermal analysis (TG-DTA) on a Rigaku standard type thermogravimetric analyzer. In a typical

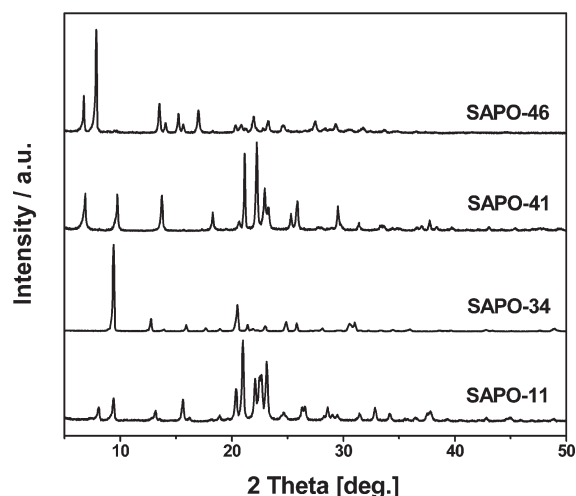


Figure 1. XRD patterns of the as-synthesized silicoaluminophosphates under study.

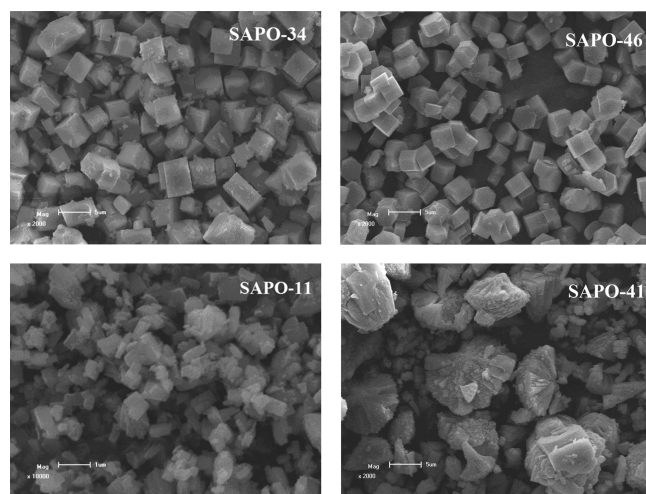


Figure 2. SEM images of SAPO-34, SAPO-41, SAPO-11, and SAPO-46.

measurement, 0.1 g of sample was heated in an Al_2O_3 crucible with a constant heating rate of 10 K/min and air purging using a flow rate of 30 mL/min.

The constitutions of occluded hydrocarbons in the different silicoaluminophosphates after the MTO reaction were analyzed by gas chromatography-mass spectrometry (GC-MS). Typically, 0.3 g of catalyst sample after reaction was carefully dissolved in 1 M HCl solution. The solution was treated with CH_2Cl_2 to extract the organic compounds and the residual water was removed by the addition of sufficient sodium sulfate solid. Then, 1.0 μL CH_2Cl_2 organic extract was analyzed by GC-MS (Agilent 7890A/5975 MSD) with a DB-5 MS column (30 m, 0.25 mm i.d., stationary phase thickness 0.25 μm). The following temperature program was employed: isothermal at 313 K for 6 min, heating to 553 K with a rate of 10 K/min, and isothermal at 553 K for 10 min.

3. RESULTS AND DISCUSSION

3.1. Physico-Chemical Properties of Silicoaluminophosphates. Figure 1 shows the powder XRD patterns of the as-

Table 2. Chemical Compositions and Surface Areas of the Calcined Silicoaluminophosphates under Study

samples	elemental analysis ^a (mmol/g)				BET surface area ^b (m^2/g)
	n_{Al}	n_{P}	n_{Si}	$n_{\text{Si}}/(n_{\text{Si}}+n_{\text{Al}}+n_{\text{P}})$	
SAPO-34	6.19	4.62	2.23	0.17	464
SAPO-41	7.27	6.81	0.50	0.03	235
SAPO-11	10.5	3.42	1.51	0.10	207
SAPO-46	7.41	5.95	2.20	0.14	242

^a Determined by ICP-AES. ^b Determined by N_2 -absorption

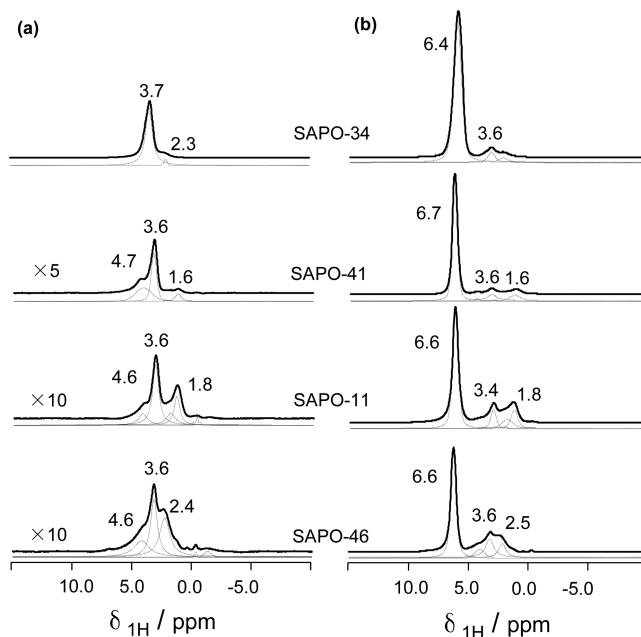


Figure 3. ^1H MAS NMR spectra of calcined silicoaluminophosphates: (a) samples dehydrated at 723 K for 12 h, (b) samples in (a) after loading with NH_3 and evacuation at 453 K for 2 h.

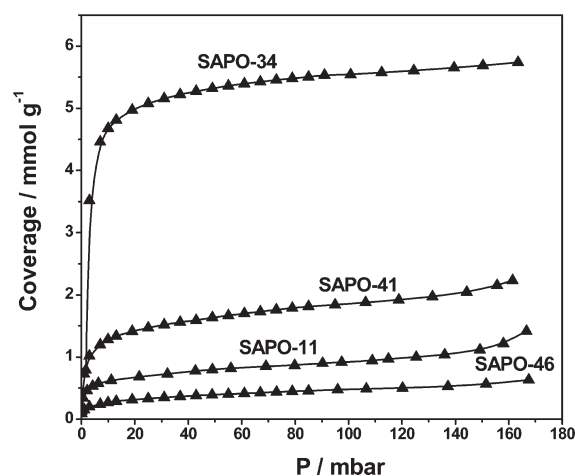
synthesized sample materials. Typical diffraction lines corresponding to CHA (SAPO-34), AFO (SAPO-41), AEL (SAPO-11), and AFS (SAPO-46) framework structures are observed,²⁷ indicating that pure phases of these topologies are obtained for the silicoaluminophosphates under study. The crystal morphologies of the as-synthesized samples were investigated by SEM. The corresponding images are shown in Figure 2. SAPO-34 crystals appear as cubes with sizes of 3–5 μm , while SAPO-41 particles have cauliflower-type congeries, which are composed of small sticks (<1 μm width and ca. 5 μm length). SAPO-11 crystals appear as cubes like SAPO-34, but the cube sizes (0.5–1 μm) are significantly smaller. SAPO-46 crystals are small symmetrical hexagonal prisms with diameters of 2–4 μm . Hence, crystals with sizes in the micrometer scale and different morphologies were observed for the silicoaluminophosphates employed in this study. The chemical composition and BET surface areas of the calcined silicoaluminophosphates are given in Table 2. The surface areas of these samples are in the range of 207 to 464 m^2/g indicating the intactness and accessibility of the pore systems.

The Brønsted acid sites of the silicoaluminophosphates under study were characterized by means of ^1H MAS NMR

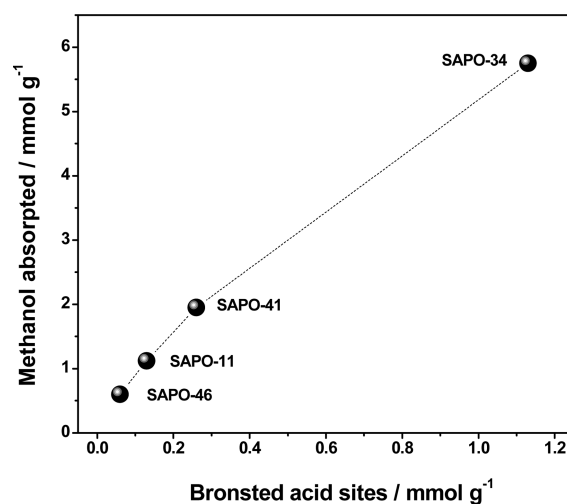
Table 3. Chemical Shifts, $\delta_{1\text{H}}$, of Si(OH)Al Groups and Ammonium Ions and Concentrations, n_{acOH} , of Brønsted Acid Sites of the Silicoaluminophosphates under Study

samples	Si(OH)Al ^a $\delta_{1\text{H}}$ /ppm	NH ₄ ^{+b} $\delta_{1\text{H}}$ /ppm	Brønsted acid sites ^c n_{acOH} /mmol g ⁻¹
SAPO-34	3.7	6.4	1.15
SAPO-41	3.6, 4.7	6.7	0.25
SAPO-11	3.6, 4.6	6.6	0.13
SAPO-46	3.6, 4.6	6.6	0.08

^a Samples dehydrated at 723 K and under a pressure below 10⁻² Pa for 12 h. ^b Samples (a) loaded with 100 mbar NH₃ at room temperature for 10 min and subsequently evacuated at 453 K for 2 h. ^c Available Brønsted acid sites (acOH) determined by ¹H MAS NMR spectroscopy

**Figure 4.** Isotherms of methanol adsorption on the silicoaluminophosphates under study.

spectroscopy. The obtained spectra are shown in Figure 3. Signals at 1.2 to 2.4 ppm are due to Si–OH, P–OH, and Al–OH groups at the outer crystal surface and framework defects,^{28,29} while signals at 3.6 to 3.7 and 4.6 to 4.7 ppm are due to bridging OH groups (Si(OH)Al), that is, Brønsted acid sites. Specifically, signals at 3.6 to 3.7 ppm indicate the presence of Si(OH)Al groups in large cages and pores, while signals at 4.6 to 4.7 ppm are assigned to Si(OH)Al groups in small structural building units and cages.^{29,30} Adsorption of the strongly basic probe molecule NH₃ on Brønsted acid sites leads to the formation of ammonium ions resulting in the appearance of ¹H MAS NMR signals at 6.0 to 7.0 ppm.^{29,30} The signal intensities of these ammonium ions are utilized for quantifying the number of accessible Brønsted acid sites (see Table 3).³¹ As indicated by the spectra of ammonia-loaded samples in Figure 3, very small fractions of Brønsted acid sites (signals at ca. 3.2 ppm) are left even after NH₃ adsorption, which are not accessible for the probe molecules and not available during the reaction. The amounts of accessible Brønsted acid sites have the sequence SAPO-34 > SAPO-41 > SAPO-11 > SAPO-46 (Table 3, column 4). The ²⁹Si MAS NMR spectra of the calcined SAPO-34 and SAPO-41 materials have strong signals at about -90 ppm attributed to Si(1Al) silicon atoms, which are a prerequisite for the formation of bridging Si(OH)Al groups (see Supporting Information, Figure S2). The simulation of the ²⁹Si MAS NMR spectra indicates that about 50% and 55% of the silicon atoms exist as Si(1Al) species causing ²⁹Si MAS NMR signals at about -90 ppm in the spectra of SAPO-34 and SAPO-41, respectively.³⁰ For SAPO-11 and SAPO-46, most of the silicon atoms exist as silica islands responsible for the signals at -100 to -115 ppm and only 11% and 4% of the silicon atoms are Si(1Al) species,

**Figure 5.** Concentrations of methanol on saturated silicoaluminophosphates plotted as a function of the amounts of accessible Brønsted acid sites in these materials.

respectively.³⁰ The amounts of accessible Brønsted acid sites are directly proportional to the silicon atoms in Si(1Al) species (see Supporting Information, Table S1). As a result of these siliceous islands, the amounts of Brønsted acid sites of SAPO-46 and SAPO-11 are much lower than those of SAPO-41 and SAPO-34.

3.2. Methanol Adsorption on Silicoaluminophosphates.

The adsorption of methanol on catalysts is one of the initial steps of methanol conversion and thus the adsorption behavior is very important for the properties of MTO catalysts. However, the adsorption of methanol on catalysts under reaction conditions is difficult to measure, for example, because of the fast coke formation. It has been demonstrated that the amount of methanol adsorbed on SAPO-34 at reaction temperature can be extrapolated from low-temperature experiments.⁹ Therefore, adsorption of methanol on silicoaluminophosphates was investigated at 298 K to gain data on their relative methanol adsorption capacities. As shown in Figure 4, the amount of methanol adsorbed on the silicoaluminophosphates under study has the sequence SAPO-34 > SAPO-41 > SAPO-11 > SAPO-46, which agrees with the behavior of the amounts of accessible Brønsted acid sites determined by ¹H MAS NMR spectroscopy (vide supra). As it is well-known, methanol adsorption on Brønsted acid sites of silicoaluminophosphates leads to the formation of strongly bound surface methoxy groups in the case of low methanol loadings, while for high methanol loadings large adsorbate complexes of weakly bound methanol molecules dominate.^{32,33} As indicated by Figure 5, the methanol concentration on saturated silicoaluminophosphates correlates well with

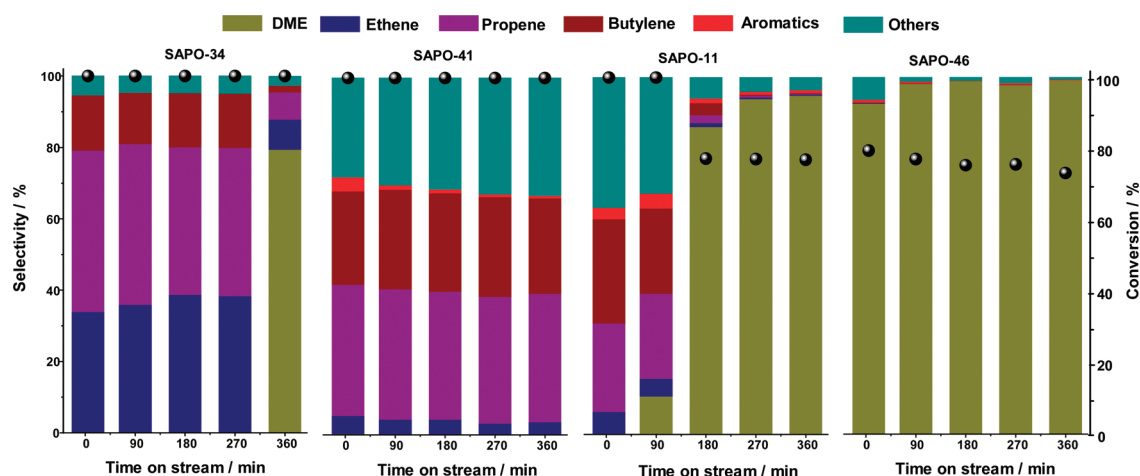


Figure 6. Methanol conversion and product selectivity during the MTO conversion on silicoaluminophosphates at 723 K up to a time-on-stream of 6 h.

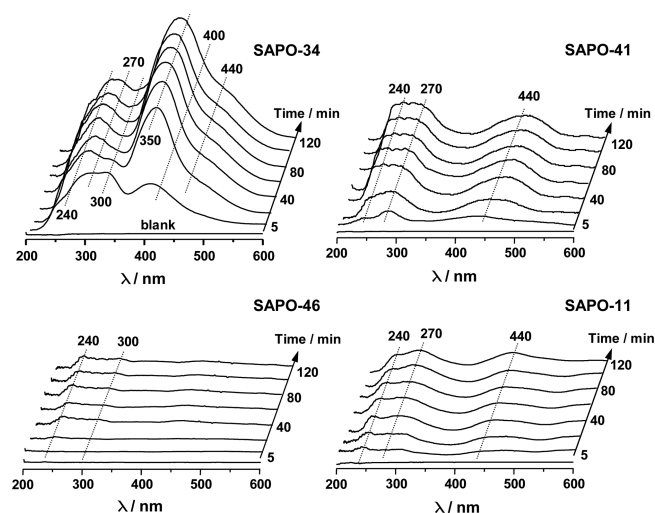


Figure 7. In situ UV/vis spectra recorded during MTO reaction on silicoaluminophosphates at 723 K and depicted as a function of the reaction time.

the concentration of accessible Brønsted acid sites determined by ^1H MAS NMR spectroscopy. For SAPO-34, about five methanol molecules are adsorbed per accessible Brønsted acid site, which fits very well with the size of methanol adsorbate complexes on acidic zeolites suggested earlier.³³

3.3. Performance of Silicoaluminophosphates in the MTO Reaction. In Figure 6, the time dependence of the methanol conversion and product selectivity during the MTO conversion on the silicoaluminophosphates under study is summarized. For SAPO-34, the selectivity to $\text{C}_2\text{--C}_4$ olefins keeps at $>95\%$ for the first 270 min of time-on-stream, which dramatically decreases to about 18% (DME: ca. 80%) after a reaction time of 360 min. During the progress of the reaction from 2 to 270 min, a gradual change of the product selectivity from propene to ethene is observed. In contrast, the selectivity to $\text{C}_2\text{--C}_4$ olefins on SAPO-41 is rather stable and maintained at about 70%, also after a time-on-stream of 360 min. Further experiments indicated that the high selectivity as well as high methanol conversion on SAPO-41 can be preserved for reaction times up to 10 h before they begin to decrease (see Supporting Information, Figure S3).

For SAPO-11, the selectivity to $\text{C}_2\text{--C}_4$ olefins is about 60% after the initial 2 min, and it gradually decreases to about 52% at the time-on-stream of 90 min. With the further extension of the methanol conversion, the selectivity to $\text{C}_2\text{--C}_4$ decreases dramatically and finally drops down to $<1\%$ after the reaction time of 360 min. In comparison with SAPO-34, much higher contents of butylene, $\text{C}_5\text{--C}_7$ aliphatics, and aromatics are present in the product mixtures formed on SAPO-11 and SAPO-41. This finding indicates the preferred formation of molecules with large dynamic diameters in the channels of these catalysts. For SAPO-46, on the other hand, the initial selectivity to light olefins is quite low, and DME is the dominant product during the MTO conversion.

3.5. In Situ UV/vis Studies of the MTO Reaction. Using in situ UV/vis spectroscopy, the nature of organic compounds formed during the MTO conversion was studied under reaction conditions. For SAPO-34, UV/vis bands at 240, 270, 300, and 400 nm appear during the initial 5 min (Figure 7). The bands at 270 and 400 nm are assigned to aromatics and polycyclic aromatics, respectively,³⁴ while the bands at 240 and 300 nm indicate the formation of dienes and monoenylic carbenium ions,³⁵ respectively. With the further progress of the reaction, monoenylic carbenium ions gradually disappear and dienylic carbenium ions (band at 350 nm³⁵) and trienylic carbenium ions (band at 440 nm³⁵) appear. These observations are a hint that olefins react with monoenylic carbenium ions to dienylic and trienylic carbenium ions on the working catalysts. Monoenylic and dienylic carbenium ions may contribute to the formation of aromatic hydrocarbon pool compounds (e.g., polyalkylaromatics), while trienylic carbenium ions may be responsible for the formation of large organic deposits (e.g., polycyclic aromatics).³⁶

For SAPO-41, dienes (band at 240 nm), aromatics (band at 270 nm), and dienylic carbenium ions (band at 450 nm) are observed after the initial 5 min. The amount of these species increases with increasing reaction time up to 40 min and remains stable thereafter. Aromatics originating from dienylic carbenium ions are the main hydrocarbon pool compounds occluded in SAPO-41.

For SAPO-11, dienes, aromatics, and dienylic carbenium ions are observed in the UV/vis spectra recorded during the MTO reaction, similar to those obtained for SAPO-41. However, the amounts of these species are much lower, probably because of the small amount of Brønsted acid sites available on SAPO-11 in comparison with SAPO-41. For SAPO-46, only traces UV/vis

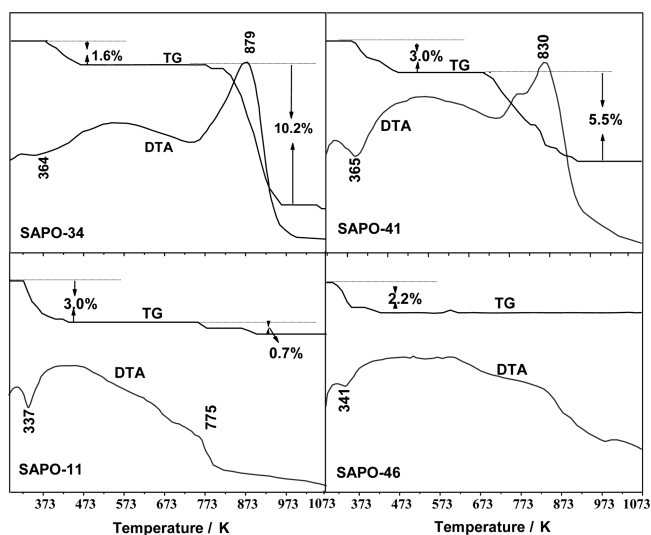


Figure 8. TG-DTA curves of spent silicoaluminophosphates obtained after MTO conversion at 723 K for 6 h.

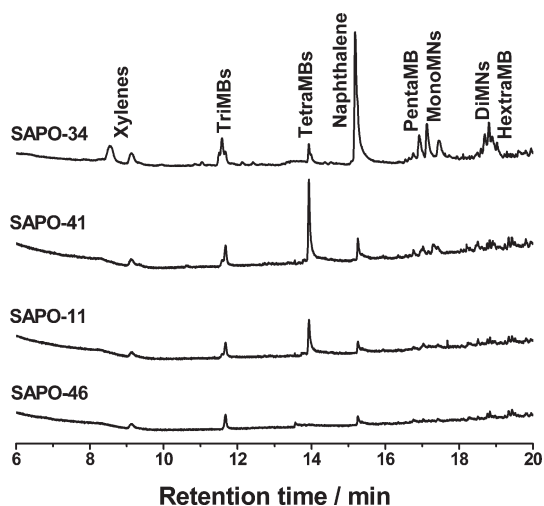


Figure 9. GC-MS analysis of occluded organic species in the silicoaluminophosphates after a MTO reaction at 723 K for 6 h.

sensitive dienes (band at 240 nm) and monoenylic carbenium ions (band at 300 nm) can be observed after a reaction time of 40 min. These monoenylic carbenium ions are not enough to form sufficient hydrocarbon pool compounds. Consequently, a very low MTO activity was found for SAPO-46.

3.5. Occluded Organic Species Formed on the Catalysts during the MTO Reaction. The results of TG-DTA studies on spent silicoaluminophosphate catalysts obtained after a reaction time of 6 h are shown in Figure 8. In general, two obvious weight losses can be recognized in the TG curves: A low-temperature weight loss at <473 K and a high-temperature weight loss at >673 K. Correspondingly, two peaks can be observed in DTA curves: A low-temperature endothermic peak and a high-temperature exothermic peak. The endothermic peak is ascribed to desorption of weakly adsorbed water and/or volatile organic compounds, while the exothermic peak is due to the oxidation of occluded carbon pool compounds. The amounts of the occluded organic compounds are 10.2%, 5.5%, and 0.7% in SAPO-34, SAPO-41, and SAPO-11, respectively. In contrast, no occluded

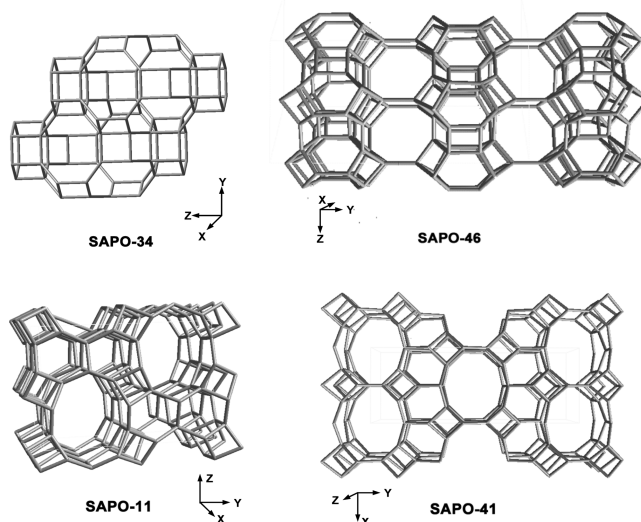


Figure 10. Illustration of framework structure of silicoaluminophosphate molecular sieves.

organic compounds were found by TG-DTA analysis for SAPO-46. These findings are in good agreement with the results of in situ UV/vis spectroscopy.

The exact constitution of the occluded hydrocarbon pool compounds in the spent catalyst samples was analyzed by GC-MS after dissolution of the catalyst framework and titration of the organics. The corresponding results are shown in Figure 9. Methylbenzenes (MBs) and methylnaphthalenes (MNs) with one to two fused aromatic rings are observed in all the samples, whereas the specific distributions of aromatics are different. For SAPO-34, the main species is naphthalene, with fewer amounts of MBs and MNs. For SAPO-41 and SAPO-11, tetraMBs are the main species, with fewer amounts of xylenes, triMBs, and naphthalene. For SAPO-46, on the other hand, the amounts of MBs and MNs are negligible, which also agree with the results of in situ UV/vis spectroscopy.

3.6. Factors Controlling the Performances of MTO Catalysts. For the MTO conversion on acidic zeolite catalysts it is generally accepted that the properties of acid sites and the microporous framework structure are key factors controlling the product distribution and catalyst deactivation.¹⁹ Therefore, the following discussion of the MTO conversion on silicoaluminophosphate catalysts focuses on these two factors.

Figure 10 illustrates the different framework structures of silicoaluminophosphates employed in this study. SAPO-34 and SAPO-46 both possess structures with cages and they are discussed in parallel, therefore. For SAPO-34, the small 8-ring windows permit the diffusion exclusively of linear hydrocarbons, whereas the diffusion of branched hydrocarbons with high carbon numbers ($C > 4$) and aromatics with large kinetic diameters is hindered. As a result, such organic compounds can not be detected in the product flow, and a high selectivity toward lower olefins is obtained (Figure 6). However, organic species with kinetic diameters much larger than the cages of SAPO-34, for example, polycyclic aromatics, can be detected by in situ UV/vis spectroscopy during the MTO conversion. Strong loading of SAPO-34 with these species leads to a blocking of the pore entrances causing a catalysts' deactivation.

For SAPO-46, on the other hand, the large cages are interconnected by 12-ring windows (diameter of ca. 0.70 nm)

permitting the diffusion of branched high-carbon hydrocarbons ($C > 4$) and alkylbenzenes, so that these organic compounds can be detected in the initial product flow (Figure 6). SAPO-34 exhibits a high MTO activity, while SAPO-46 shows a quite low activity in the olefin production. ^1H MAS NMR spectroscopic studies of samples loaded with ammonia revealed that SAPO-34 possesses 1.15 mmol/g accessible Brønsted acid sites, while SAPO-46 possesses the much lower amount of 0.08 mmol/g of these surface sites (Table 3, column 4). Furthermore, the results of in situ UV/vis spectroscopy and GC-MS indicate that a large amount of polyalkylbenzenes and polycyclic aromatics are occluded in SAPO-34, while only a small amount of polyalkylbenzenes is formed on SAPO-46. According to the generally accepted reaction mechanism, large hydrocarbon pool compounds are the key intermediates for the formation of olefins from the methanol/DME reactant mixture.^{10,11} In the case of SAPO-46, however, the amount of available Brønsted acid sites is too low for the formation of sufficient hydrocarbon pool compounds. As a result, no olefins are formed, and DME is detected as the main reaction product.

SAPO-41 and SAPO-11 possess similar one-dimensional 10-ring pores with sizes of 0.40×0.65 nm and 0.43×0.70 nm,³⁷ respectively. Polyalkylbenzenes and branched high-carbon hydrocarbons can diffuse through these 10-ring pores and, correspondingly, they are detected in product flow (Figure 6). After a longer time-on-stream, polyalkylbenzenes are occluded also in SAPO-41 and SAPO-11 (Figures 7 and 9) although the diffusion of polyalkylbenzenes is not hindered at all. This finding may indicate that the negative framework charges occurring upon deprotonation of Brønsted acid sites may stabilize nearby carbenium ions, which act as intermediates in the formation of polyalkylbenzenes.

SAPO-41 and SAPO-11 both exhibit a remarkable initial MTO activity. However, the activity sharply decreases after a time-on-stream of 90 min for SAPO-11. In contrast, the activity of SAPO-41 is well-preserved up to a reaction time of 10 h. The results of in situ UV/vis spectroscopy, TG-DTA, and GC-MS indicate that much less organic species are occluded in SAPO-11 after a time-on-stream of 6 h than in SAPO-41 after the same reaction time. The amounts of coke occluded in SAPO-11 and SAPO-41 are 0.7% and 5.5%, respectively. Hence, the deactivation of SAPO-11 is not caused by the formation of organic deposits acting as coke. ^1H MAS NMR spectroscopic results reveal that SAPO-41 possesses much more Brønsted acid sites (0.25 mmol/g) than SAPO-11 (0.13 mmol/g), but the in situ UV/vis investigations (Figure 7) indicate that carbenium ions are formed both on SAPO-41 and SAPO-11. On SAPO-11, these carbenium ions cover the few existing Brønsted acid sites, which are required for the MTO reaction.³⁸ Therefore, deactivation of the SAPO-11 occurs if not sufficient Brønsted acid sites are left. On the other hand, the selectivity of SAPO-11 and SAPO-41 to ethene is much lower than that of SAPO-34, but the selectivities to propylene and butylene are higher, which is very similar to catalytic performance of ZSM-5. From this point, the mechanism of the MTO conversion on SAPO-11 and SAPO-41 should be more similar to ZSM-5 rather than SAPO-34, that is, ethene is formed from the lower methylbenzenes followed by remethylation, and C_{3+} alkenes are formed from a methylation/cracking cycle.^{39,40} Further researches on the routes of olefins production on SAPO-41 are underway.

Summarizing, it can be stated that the amount of Brønsted acid sites has large effect on the methanol adsorption capacity of

silicoaluminophosphates, which is important for the initiation of the MTO reaction. Additionally, the Brønsted acid sites play a key role in controlling the activity and lifetime of the MTO catalysts. On one side, the Brønsted acid sites favor the formation of hydrocarbon pool compounds and, correspondingly, a high methanol conversion is obtained on catalysts with a high concentration of these catalytically active surface sites. On the other side, a large concentration of Brønsted acid sites favors the further condensation of hydrocarbon pool compounds, which results in the formation of coke deposits causing catalyst deactivation, for example, in the case of SAPO-34. Furthermore, the available Brønsted acid sites are gradually involved in the formation and stabilization of carbenium ions, and deactivation of the catalysts may also occur if there are not sufficient Brønsted acid sites left, for example, in the case of SAPO-11. Finally, the different pore architectures of the silicoaluminophosphates studied in the present work influence the diffusion of the reaction products and thus control the product selectivity in the MTO reaction. Small pores and windows favor light olefins with small dynamic diameters (SAPO-34) in the product mixture, whereas large pores lead to products with large dynamic diameters (SAPO-11 and SAPO-41).

4. CONCLUSIONS

In the present study, several types of silicoaluminophosphates with different framework structures having different pore systems and properties of Brønsted acid sites were synthesized and studied as MTO catalysts. Distinct catalytic performances, including the selectivity to light olefins and catalyst deactivation were observed for these materials. The Brønsted acid sites of silicoaluminophosphates influence the methanol adsorption and the catalyst activity as well as the lifetime of the catalysts in the MTO reaction, while the pore architecture mainly influences the product distribution and reaction routes. Therefore, SAPO-41 with one-dimensional 10-ring pores and a significant concentration of Brønsted acid sites also exhibits good MTO activity. For this material, methanol conversion of 100% and a selectivity to light olefins of about 70% are achieved maintaining for a time-on-stream of 10 h at the reaction temperature of 723 K. Moreover, the well-defined pore structure of SAPO-41 and the limited number of hydrocarbon pool compounds acting as reaction intermediates make this material to an interesting candidate for further mechanistic studies of the MTO reaction.

■ ASSOCIATED CONTENT

Supporting Information. Scheme of in situ UV/vis spectroscopy, ^{29}Si MAS NMR spectra of silicoaluminophosphates, methanol conversion and product selectivity of SAPO-41 with a time-on-stream of 10 h are supplied as described in the text (PDF). This material is available free of charge via the Internet at <http://pubs.acs.org>.

■ AUTHOR INFORMATION

Corresponding Author

*E-mail: lild@nankai.edu.cn. Fax: +86-22-2350-0341. Phone: +86-22-2350-0341.

■ ACKNOWLEDGMENT

This work is supported by the National Basic Research Program of China (2009CB623502) and MOE (IRT0927). Furthermore,

M.H. wants to thank for financial support by Fonds der Chemischen Industrie and Deutsche Forschungsgemeinschaft.

REFERENCES

- (1) Chang, C. D. *Catal. Rev. Sci. Eng.* **1983**, *25*, 1–118.
- (2) Chang, C. D. *Catal. Rev. Sci. Eng.* **1984**, *26*, 323–345.
- (3) Stöcker, M. *Microporous Mesoporous Mater.* **1999**, *29*, 3–48.
- (4) Haw, J. F.; Song, W.; Marcus, D. M.; Nicholas, J. B. *Acc. Chem. Res.* **2003**, *36*, 317–326.
- (5) Olsbye, U.; Bjørgen, M.; Svelle, S.; Lillerud, K. P.; Kolboe, S. *Catal. Today* **2005**, *106*, 108–111.
- (6) Wilson, S.; Barger, P. *Microporous Mesoporous Mater.* **1999**, *29*, 117–126.
- (7) Dahl, I. M.; Kolboe, S. *J. Catal.* **1994**, *149*, 304–309.
- (8) Dahl, I. M.; Kolboe, S. *J. Catal.* **1996**, *161*, 458–464.
- (9) Chen, D.; Rebo, H. P.; Moljord, K.; Holmen, A. *Ind. Eng. Chem. Res.* **1999**, *38*, 4241–4249.
- (10) Song, W.; Haw, J. F.; Nicholas, J. B.; Heneghan, C. S. *J. Am. Chem. Soc.* **2000**, *122*, 10726–10727.
- (11) Song, W.; Fu, H.; Haw, J. F. *J. Am. Chem. Soc.* **2001**, *123*, 4749–4754.
- (12) Song, W.; Marcus, D. M.; Fu, H.; Ehresmann, J. O.; Haw, J. F. *J. Am. Chem. Soc.* **2001**, *124*, 3844–3845.
- (13) Wu, X.; Abraha, M. G.; Anthony, R. G. *Appl. Catal., A* **2004**, *260*, 63–69.
- (14) Lee, Y. J.; Baek, S. C.; Jun, K. W. *Appl. Catal., A* **2007**, *329*, 130–136.
- (15) Hereijgers, B. P. C.; Bleken, F.; Nilsen, M. H.; Svelle, S.; Lillerud, K. P.; Bjørgen, M.; Weckhuysen, B. M.; Olsbye, U. *J. Catal.* **2009**, *264*, 77–87.
- (16) Bleken, F.; Bjørgen, M.; Palumbo, L.; Bordiga, S.; Svelle, S.; Lillerud, K. P.; Olsbye, U. *Top. Catal.* **2009**, *52*, 218–228.
- (17) Marcus, D. M.; Song, W.; Ng, L. L.; Haw, J. F. *Langmuir* **2002**, *18*, 8386–8391.
- (18) Gayubo, A. G.; Aguayo, A. T.; Alonso, A.; Atutxa, A.; Bilbao, J. *Catal. Today* **2005**, *106*, 112–117.
- (19) Aguayo, A. T.; Gayubo, A. G.; Vivanco, R.; Olazar, M.; Bilbao, J. *Appl. Catal., A* **2005**, *283*, 197–207.
- (20) Djieugoue, M. A.; Prakash, A. M.; Kevan, L. *J. Phys. Chem. B* **2000**, *104*, 6452–6461.
- (21) Zhu, Z.; Hartmann, M.; Kevan, L. *Chem. Mater.* **2000**, *12*, 2781–2787.
- (22) Castro, M.; Warrender, S. J.; Wright, P. A.; Apperley, D. C.; Belmabkhout, Y.; Pirngruber, G.; Min, H. K.; Park, M. B.; Hong, S. B. *J. Phys. Chem. C* **2009**, *113*, 15731–15741.
- (23) Tan, J.; Liu, Z.; Bao, X.; Liu, X.; Han, X.; He, C.; Zhai, R. *Microporous Mesoporous Mater.* **2002**, *53*, 97–108.
- (24) Kong, W.; Dai, W.; Li, N.; Guan, N.; Xiang, S. *J. Mol. Catal. A* **2009**, *308*, 127–133.
- (25) Murthy, K. V. V. S. B. S. R.; Kulkarni, S. J. S. K. *Microporous Mesoporous Mater.* **2001**, *43*, 201–209.
- (26) Jiang, Y.; Huang, J.; Weitkamp, J.; Hunger, M. *Stud. Surf. Sci. Catal.* **2007**, *170*, 1137–1144.
- (27) *Collection of simulated XRD powder patterns for zeolites*, 5th revised ed.; Treacy, M. M. J., Higgins, J. B., Eds.; Elsevier: Oxford, 2007.
- (28) Hunger, M. *Catal. Rev. Sci. Eng.* **1997**, *39*, 345–393.
- (29) Hunger, M.; Anderson, M. W.; Ojo, A.; Pfeifer, H. *Microporous Mater.* **1993**, *1*, 17–32.
- (30) Buchholz, A.; Wang, W.; Xu, M.; Arnold, A.; Hunger, M. *Microporous Mesoporous Mater.* **2002**, *56*, 267–278.
- (31) Huang, J.; van Vegten, N.; Jiang, Y.; Hunger, M.; Baiker, A. *Angew. Chem., Int. Ed.* **2010**, *49*, 7776–7781.
- (32) Wang, W.; Hunger, M. *Acc. Chem. Res.* **2008**, *41*, 895–904.
- (33) Anderson, M. W.; Barrie, P. J.; Klinowski, J. *J. Phys. Chem.* **1991**, *95*, 235–239.
- (34) Crews, P.; Rodriguez, J.; Jaspars, M. *Organic Structure Analysis*; Oxford University Press: New York, 1998.
- (35) Kirisci, I.; Förster, H.; Tasi, G.; Nagy, J. B. *Chem. Rev.* **1999**, *99*, 2085–2114, and references therein.
- (36) Jiang, Y.; Huang, J.; Marthala, V. R. R.; Ooi, Y. S.; Weitkamp, J.; Hunger, M. *Microporous Mesoporous Mater.* **2007**, *105*, 132–139.
- (37) Baerlocher, Ch.; Meier, W. M.; Olson, D. H. *Atlas of zeolite framework types*, 5th revised ed.; Elsevier: Amsterdam, The Netherlands, 2007.
- (38) Yang, S.; Kondo, J. N.; Domen, K. *Catal. Today* **2002**, *73*, 113–125.
- (39) Svelle, S.; Joensen, F.; Nerlov, J.; Olsbye, U.; Lillerud, K. P.; Kolboe, S.; Bjørgen, M. *J. Am. Chem. Soc.* **2006**, *128*, 14770–14771.
- (40) Bjørgen, M.; Svelle, S.; Joensen, F.; Nerlov, J.; Kolboe, S.; Bonino, F.; Palumbo, L.; Bordiga, S.; Olsbye, U. *J. Catal.* **2007**, *249*, 195–207.